



Alternative algorithms for simultaneous modeling of ordering and intermediate compound growth during reactive diffusion

Viktoriia Pasichna^{*}, Andriy Gusak

The Bohdan Khmelnytsky National University of Cherkasy, Ukraine

ARTICLE INFO

Keywords:

Diffusion
Ordering
Intermediate phase
Phase growth
Monte Carlo simulation
Metropolis algorithm
Residence Time Algorithm
BCC-lattice
FCC-lattice
Kinetics

ABSTRACT

Standard Monte Carlo algorithms with constant pair interactions within the first coordination shell are usually quite effective for the description of ordering, tracer diffusion, chemical diffusion (but without Kirkendall shift effect) within any already existing ordered intermediate phase. Yet, one encounters big problems if one tries to simulate the formation and growth of ordered intermediate phase or, especially, simultaneous formation and growth of several intermediate phases during interdiffusion. Two algorithms providing solution of this problem, are discussed. The first algorithm is known (but not widely used for reactive growth) – account of interactions in the two coordination shells with negative mixing energy in the first coordination shell and positive mixing energy in the second one. The second algorithm is new: interactions only within the first coordination shell of each atom but depending on the local composition within the cluster around interacting atoms. Both algorithms are shown to provide formation and growth of the ordered intermediate phases with rather narrow concentration ranges, growing with time (after some initial period) according to parabolic law.

1. Introduction

Formation and growth of the ordered intermediate phases (compounds) IMC is a typical phenomenon in soldering, brazing, welding, and other ways of bonding by solid-state reactions. These processes are, typically, diffusion-controlled and need atomic migration over the crystalline lattice. Long-term properties of intermetallic reactive growth (like parabolic law, Arrhenius law) are known for many years. On the other hand, early stages of reactive diffusion still represent a big challenge both for experimental and theoretical researchers. This challenge includes the prediction of incubation time (nucleation problem), growth and suppression criteria (competition problem), the role of grain structure, and grain boundary migration (defect problem) [1]. To solve this problem, we need a simulation technique that enables simultaneous observation of atomic-scale migration, ordering, formation, and growth of ordered phases with distinct interfaces. Standard kinetic Monte-Carlo approach works very well for modeling tracer diffusion and chemical diffusion within solid solutions and ordered alloys, also for modeling of ordering in initially homogeneous alloys [2–4], but it encounters problems in application to formation and growth of intermediate order phases in diffusion couples with distinct boundaries (interfaces) between them. For example, if one tries to model formation and growth of

B2 compound at the contact of two BCC-materials, or of L1₀ compound at the contact of two FCC-materials, one gets the concentration profiles (Fig. 1a,b) which are very far from typical experimental step-wise concentration profiles of the binary couples with growing ordered IMCs. A similar difficulty is encountered by the self-consistent nonlinear kinetic mean-field (KMF method) in the version suggested by George Martin [5], developed by Erdelyi et al [6] and later generalized to the full 3D scheme [7] and the inclusion of stochastic terms [8].

Experimental curves show typical concentration plateau in the vicinity of stoichiometric concentration and two concentration steps between this plateau and terminal alloys – solution A in B and B in A [9]. Contrary to this picture, standard kinetic Monte-Carlo methods lead to continuous concentration profiles without steps and plateau. (Some steps at the final curve for L1₀-order at the right Fig. 2b are caused by the formation of antiphase L1₀-domains.)

In the couple of two FCC-materials, a standard kinetic Monte-Carlo may demonstrate three intermediate ordered phases A3B (L1₂ structure), AB (L1₀ structure), AB3(L1₂ structure), but these structures are separated with so small concentration intervals that it is sometimes a problem to distinguish the phases and to find the interfaces between them. (See for example Fig. 4 in [10].)

Up to now, to the best of our knowledge, the only way to make MC-

^{*} Corresponding author.

E-mail address: pasichna.vika2803@gmail.com (V. Pasichna).

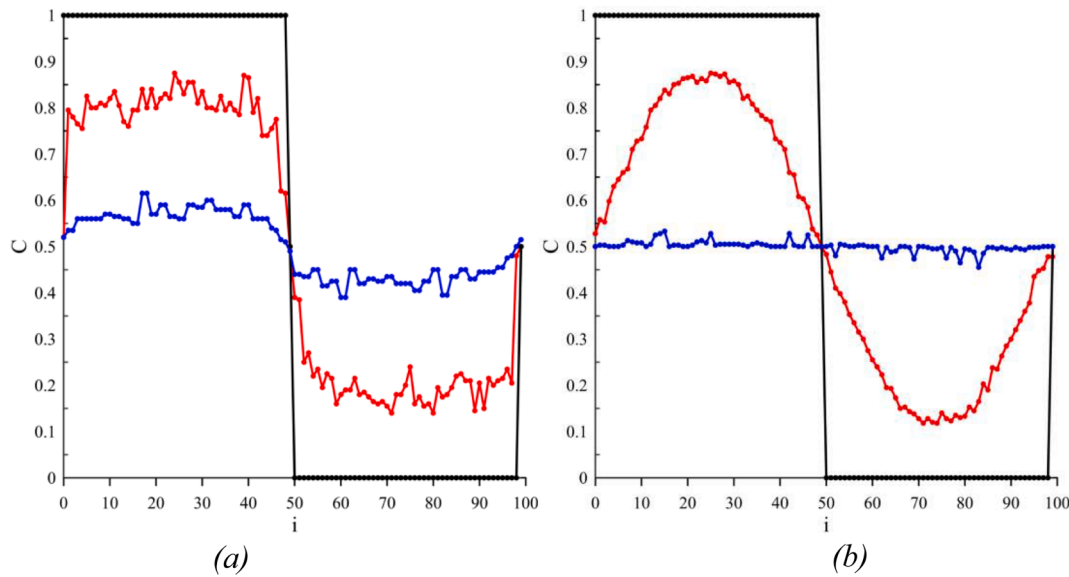


Fig. 1. Typical concentration profile evolution (averaged over YZ atomic planes) in the diffusion couple of (a) two BCC-materials with B2 ordered phase formation and (b) two FCC-materials with the formation of three ordered phases – A3B and AB3 with $L1_2$ structure, and AB with $L1_0$ -structure, simulated by Monte Carlo method with the account of only first coordination shell in the interaction energy.

profiles closer to the realistic case was an account of interaction in the second coordination shell. [8,11]. This approach is good (and we explain it below), but it needs the introduction of additional parameters for the second shell (to provide really distinct ordered phases, one needs negative mixing energy for the first shell and positive mixing energy for the second shell). In this work we suggest one more alternative method, also providing distinct ordered phases. Namely, we suggest to use the interactions only with the nearest neighbors, but with energies depending on the averaged composition in the local surrounding of the two interacting atoms. (Something similar, but in a different form, was suggested in [12]). In this work, we check this method for the simplest cases of the single intermediate compound (IMC), growing between terminal solutions, and for two competing IMCs. The idea of energy depending of local surroundings has some analogy with Hume-Rothery phases which exist at some special ratio of free electrons number per atom in the alloy. The idea of concentration-dependent interaction energies was recently used in [13]. Moreover, the influence of local surrounding on the interaction energy and the interactions within second coordination shell naturally appears when one uses the many-particle potentials in the diffusion modelling [14]

In this paper, we formulate the new method of atomistic modeling of the reactive diffusion with interatomic interactions depending on local composition in the neighborhood of both interacting atoms. We realized this method in Monte Carlo techniques and apply it to BCC and FCC lattice, using two alternatives – Metropolis algorithm for the mechanism of direct atomic exchanges and Residence-Time-Algorithm (RTA) for the vacancy mechanism. So far, we will make our tests only for the case of single growing phase B2 in BCC case and two simultaneously forming phases ($L1_0$ and $L1_2$) in the FCC case.

In Section 2 we introduce the concept of the “Local Long-range Order” for the substantially inhomogeneous systems with FCC or BCC lattices. In Section 3 we analyze the simulation of reactive diffusion with account of interactions in the second coordination shell. In Section 4 we analyze the alternative method of interactions account, dependent on local surrounding.

The simulations in Sections 3 and 4 are made under the assumptions of direct exchange mechanism and Metropolis algorithm. In Section 5 we repeat some of the simulations from Sections 3 and 4 using “true kinetic” RTA-algorithm with vacancy mechanism and compare the results with the simulations using Metropolis algorithm with direct atomic

exchange. We should note that in case of vacancy mechanism, one encounters the well-known problem of Kirkendall effect, which is still a problem for Monte Carlo simulations on the rigid lattices (except recent attempts by Sowa and Kozubski [16], which are interesting but, so far, not discussed sufficiently by diffusion community).

2. Concept of “Local Long-Range Order”(LLRO)

In globally homogeneous binary alloy, the common Long Range Order (LRO) is defined in Eq. (1):

$$\eta = \frac{p_A^I - C_A}{1 - \nu^I} \quad (1)$$

where $p_A^I = \frac{N_A^I}{N^I}$ — is the *a priori* probability of finding the A-atoms in the arbitrarily chosen lattice site of the sublattice I. N^I, N_A^I — the total number of sublattice I sites in the ordered domain and number of A-atoms on this sublattice, $C_A = \frac{N_A^I + N_A^{II}}{N^I + N^{II}}$ — a local atomic fraction of A, averaged over both sublattices (we use to call it local concentration or local composition); $\nu^I = \frac{N^I}{N^I + N^{II}}$ is the fraction of sublattice I sites.

In this paper, we consider the ordering in the sharply inhomogeneous contact zone with a rather sharp concentration gradient. In this case, the notions of the global order as well as of global composition have no sense. Instead of order parameter for the whole ordered domain, we introduce the local parameters of composition and order, introduced for each site “i” (actually, “i” denotes three coordinates of the site) within some minimal cluster of neighboring sites “in” around this fixed site “i”. The starting notion is $C_A(i)$. In Monte Carlo modeling it is equal to just 1 if the site “i” is occupied by A-atom, and it is equal just to 0 if it is occupied by B-atom. In mean-field models [5] it is a probability of site “i” to be occupied by sort A. A more detailed discussion can be found in [17].

2.1. B2-phase of BCC-lattice

In the case of inhomogeneous B2-phase of BCC-lattice (with 8 nearest neighbors and the elementary cell containing 2 sites) the local composition (averaged over the cell containing “central” atom and, partially, its nearest neighbors, which are “shared” with other cells) is defined in Eq. (2):

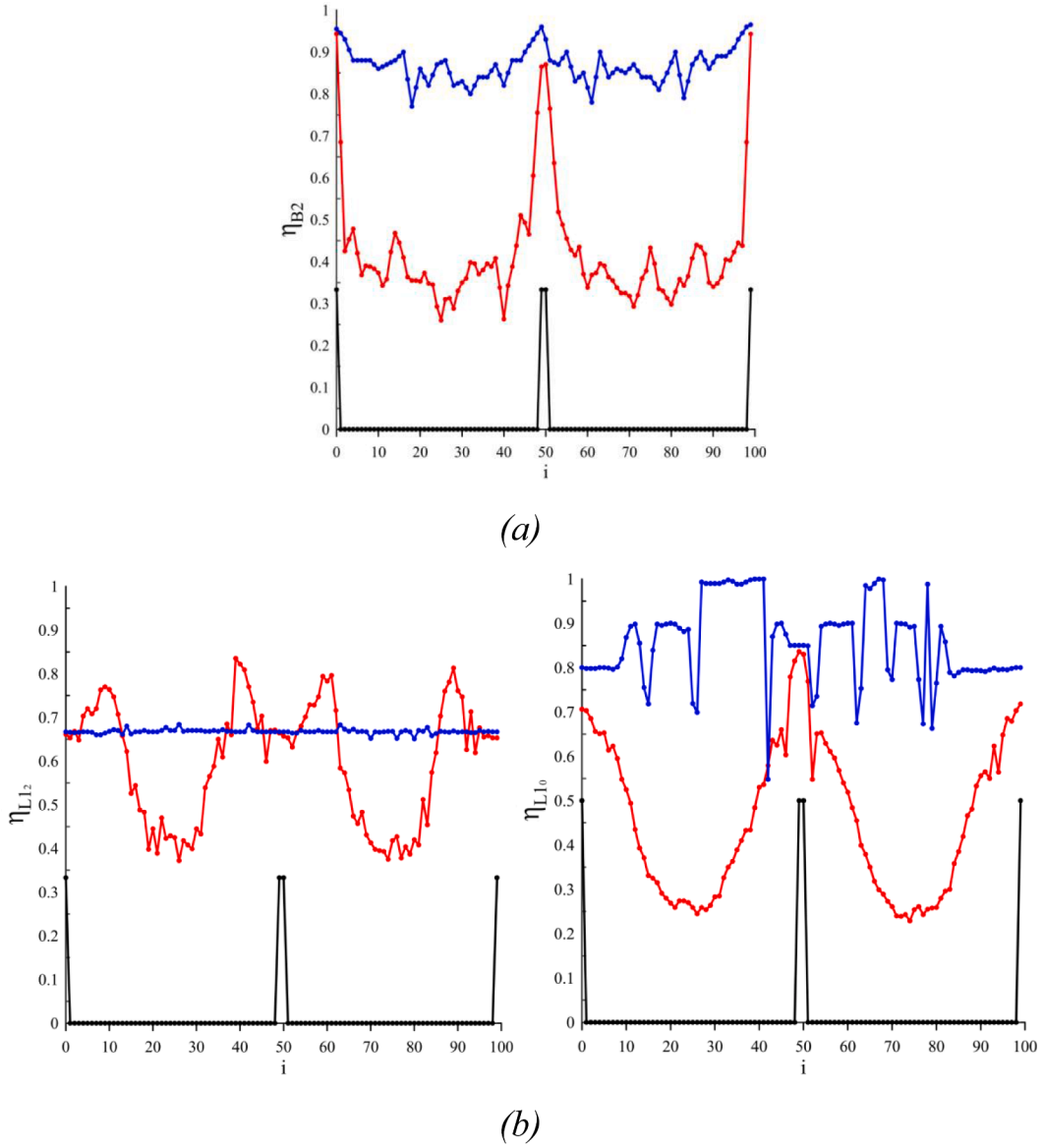


Fig. 2. Typical local order profile evolution (averaged over YZ atomic planes) in the diffusion couple of (a) two BCC-materials with B2 ordered phase formation and (b) two FCC-materials with the formation of three ordered phases – A3B and AB3 with L1₂ structure, and AB with L1₀-structure, simulated by Monte Carlo method with the account of only first coordination shell in the interaction energy. Local order was calculated by averaging over YZ-planes of Eq. (3) for B2-order at BCC-lattice, Eq. (5) for L1₂-order and Eq. (7) for L1₀-order at FCC-lattice. Steps at the final curve for L1₀-order at the right Fig. 2b are caused by the formation of antiphase L1₀-domains.

$$\bar{C}_A^{B2}(i) = \frac{C_A(i) + \frac{1}{8} \sum_{in=1}^8 C_A(in)}{2} \quad (2)$$

local a priori probability depends on the sublattice to which the site “i” belongs:

$$p_A(i) = C_A(i)$$

and

$$\eta(i) = \frac{C_A(i) - \frac{C_A(i) + \frac{1}{8} \sum_{in=1}^8 C_A(in)}{2}}{1 - 1/2} = C_A(i) - \frac{1}{8} \sum_{in=1}^8 C_A(in)$$

(if “i” belongs to sublattice A)

or

$$p_A(i) = \frac{1}{8} \sum_{in=1}^8 C_A(in)$$

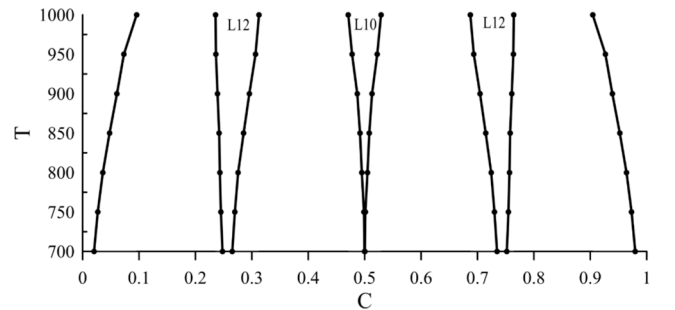


Fig. 3. Phase diagram of FCC-binary alloy with interactions within two coordination shells, calculated by MC diffusion couple method with $V_{mix}^I = -2.9 \cdot 10^{-21} J$, $V_{mix}^{II} = +6.76 \cdot 10^{-21} J$.

and

$$\eta(i) = \frac{\frac{1}{8} \sum_{in=1}^8 C_A(in) - \frac{C_A(i) + \frac{1}{8} \sum_{in=1}^8 C_A(in)}{2}}{1 - 1/2} = - \left(C_A(i) - \frac{1}{8} \sum_{in=1}^8 C_A(in) \right)$$

(if “i” belongs to sublattice B)

Thus, in general case the LLRO for inhomogeneous B2 structure is

$$\eta^{B2}(i) = \text{abs} \left(C_A(i) - \frac{1}{8} \sum_{in=1}^8 C_A(in) \right) \quad (3)$$

2.2. L1₀-phase of FCC-lattice

In the case of L1₀ phase of FCC-lattice (with 12 nearest neighbors and with elementary cell containing 4 sites) the local composition is determined by Eq. (4):

$$\bar{C}_A^{L10}(i) = \frac{C_A(i) + \frac{1}{4} \sum_{in=1}^{12} C_A(in)}{4} \quad (4)$$

Local *a priori* probability depends on sublattice orientation choice – in the XY-plane, or YZ, or ZX:

$$p_A^{XY}(i) = \frac{C_A(i) + \frac{1}{4} \sum_{in=1}^4 C_A(in/YX - plane)}{2}$$

$$p_A^{YZ}(i) = \frac{C_A(i) + \frac{1}{4} \sum_{in=1}^4 C_A(in/YZ - plane)}{2}$$

$$p_A^{ZX}(i) = \frac{C_A(i) + \frac{1}{4} \sum_{in=1}^4 C_A(in/ZX - plane)}{2}$$

$$\begin{aligned} \eta^{XY}(i) &= \left(\frac{C_A(i) + \frac{1}{4} \sum_{in=1}^4 C_A(in/YX - plane)}{2} - \frac{C_A(i) + \frac{1}{4} \sum_{in=1}^{12} C_A(in)}{4} \right) / \left(1 - \frac{1}{2} \right) = \\ &= \frac{C_A(i)}{2} + \frac{\sum_{in=1}^4 C_A(in/YX - plane)}{4} - \frac{\sum_{in=1}^{12} C_A(in)}{8} = \\ &= \frac{C_A(i)}{2} - \frac{\sum_{in=1}^4 C_A(in/YZ - plane) + \sum_{in=1}^4 C_A(in/ZX - plane) - \sum_{in=1}^4 C_A(in/YX - plane)}{8} \end{aligned}$$

$$\eta^{YZ}(i) = \frac{C_A(i)}{2} - \frac{\sum_{in=1}^4 C_A(in/ZX - plane) + \sum_{in=1}^4 C_A(in/YX - plane) - \sum_{in=1}^4 C_A(in/YZ - plane)}{8}$$

$$\eta^{ZX}(i) = \frac{C_A(i)}{2} - \frac{\sum_{in=1}^4 C_A(in/YX - plane) + \sum_{in=1}^4 C_A(in/YZ - plane) - \sum_{in=1}^4 C_A(in/ZX - plane)}{8}$$

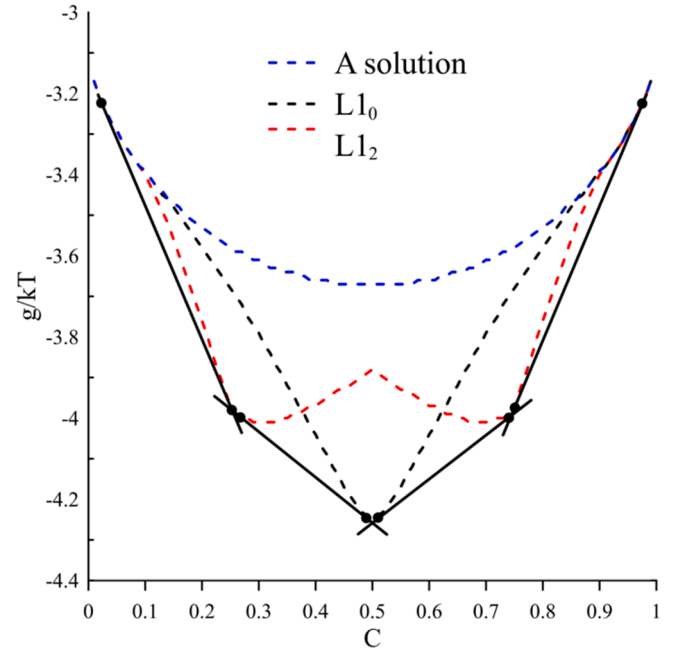


Fig. 4. Concentration dependences of Gibbs free energy per atom for three intermediate phases and for terminal solid solutions at temperature $T = 750K$, and the common tangents construction demonstrating huge concentration gaps typical for the majority of phase diagrams. Parameters: $V_{mix}^I = -2.9 \cdot 10^{-21} J$, $V_{mix}^{II} = +6.76 \cdot 10^{-21} J$.

In general, taking into account the possibilities of antiphase domains choice,

$$\eta^{L10}(i) = \max\{abs(\eta^{XY}(i)), abs(\eta^{YZ}(i)), abs(\eta^{ZX}(i))\} \quad (5)$$

2.3. L1₂-phase of FCC-lattice

Structure L1₂ corresponds approximately to A3B compound at FCC-lattice with majority sublattice I consisting of face centers (6/2 = 3 per elementary cell of 4 totals sites) and minority sublattice II consisting of vertexes (8/8 = 1 per elementary cell). The local composition is determined in the same way for any site in Eq. (6):

$$\bar{C}_A^{L12}(i) = \frac{C_A(i) + \frac{1}{4}\sum_{in=1}^{12} C_A(in)}{4} \quad (6)$$

As for local probability, its explicit expression depends on the choice (one of four possible choices) and on the orientation of plane containing the nearest neighbors from minority sublattice.

If site “i” of majority sublattice I belongs to the XY-face of the elementary cell, then it has 4 nearest neighbors from sublattice II within this plane and another 8 = 4 + 4 nearest neighbors from its own sublattice within planes YZ and ZX.

$$\begin{aligned} p_A^{XY}(i) &= \frac{C_A(i) + \frac{1}{4}\sum_{in=1}^8 C_A(in/YZ + ZX)}{3} = \frac{C_A(i) + \frac{1}{4}\sum_{in=1}^{12} C_A(in)}{3} - \frac{1}{12}\sum_{in=1}^4 C_A(in/XY) = \\ &= \frac{4}{3}\bar{C}_A(i) - \frac{1}{12}\sum_{in=1}^4 C_A(in/XY)p_A^{YZ}(i) = \frac{4}{3}\bar{C}_A(i) - \frac{1}{12}\sum_{in=1}^4 C_A(in/YZ)p_A^{ZX}(i) = \frac{4}{3}\bar{C}_A(i) - \frac{1}{12}\sum_{in=1}^4 C_A(in/ZX) \end{aligned}$$

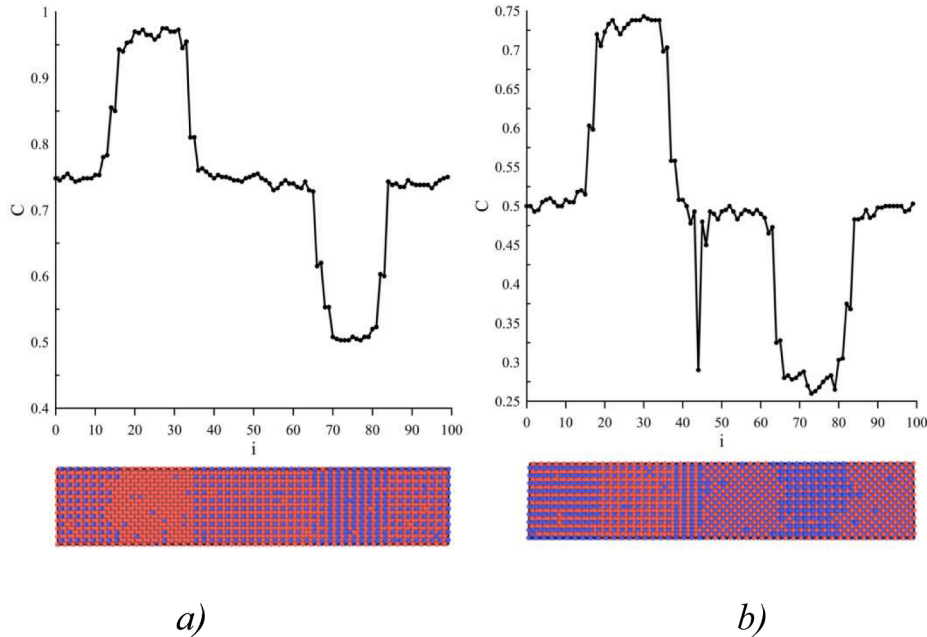


Fig. 5. Typical concentration profiles (averaged over YZ-planes) and snapshots of sites occupancy obtained by MC-simulations during diffusion and ordering in the couples: a) A-AB; b) A3B-AB3 with FCC-structure. (Interactions within two coordination shells. Parameters: $V_{mix}^I = -2.9 \cdot 10^{-21} J$, $V_{mix}^{II} = +6.76 \cdot 10^{-21} J$, $T = 750K$.)

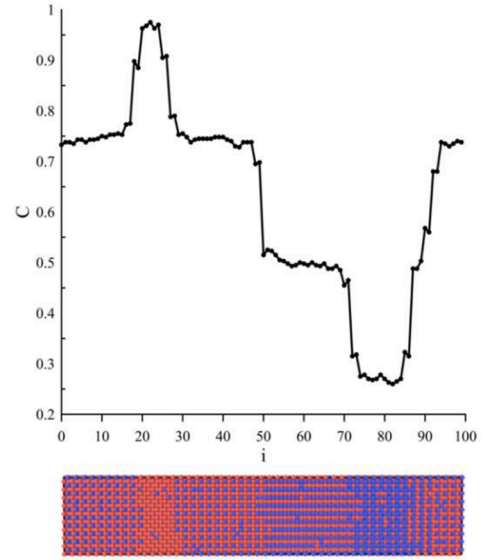


Fig. 6. Typical concentration profile (averaged over YZ-planes) and a snapshot of sites occupancy obtained by MC-simulations during diffusion and ordering in the couple A-AB3 with FCC-structure (Interactions within two coordination shells. Parameters: $V_{mix}^I = -2.9 \cdot 10^{-21} J$, $V_{mix}^{II} = +6.76 \cdot 10^{-21} J$, $T = 750K$.) Two ordered intermediate phases A3B and AB are growing simultaneously.

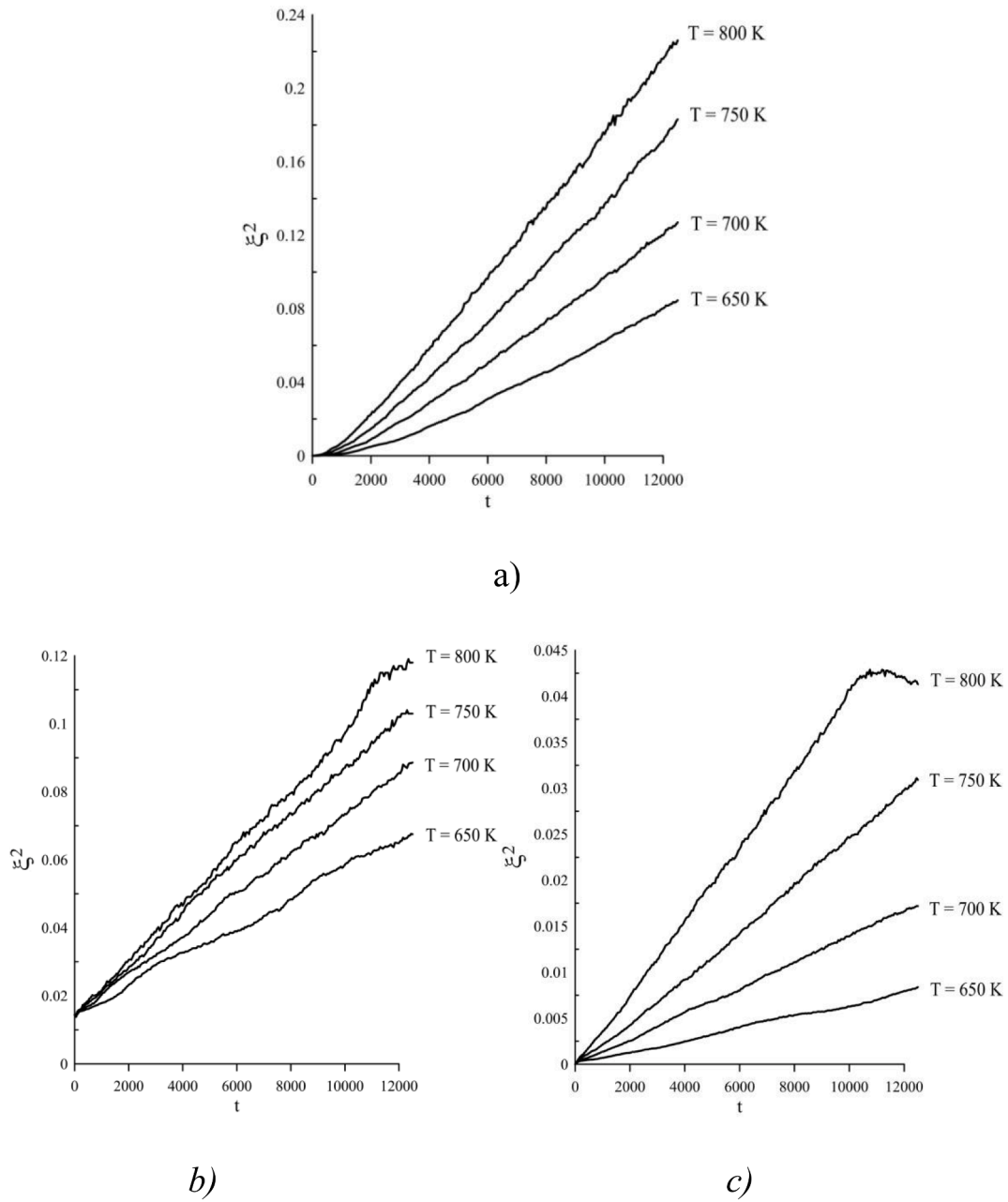


Fig. 7. Dependencies of squared fraction ξ^2 of sites with overcritical local order parameter (a) $L1_2$ in diffusion couple A-AB, (b) $L1_2$ and (c) $L1_0$ in simulation of interdiffusion between pure A and ordered AB3 at various temperatures on Monte Carlo Steps.

Thus,

$$\eta_i^{XY}(i) = \frac{p_A^{XY}(i) - C_A(i)}{1 - 3/4} = \frac{4}{3} \left(\bar{C}_A(i) - \frac{1}{4} \sum_{in=1}^4 C_A(in/XY) \right) = \frac{1}{3} \left(C_A(i) + \frac{1}{4} \sum_{in=1}^{12} C_A(in) - \sum_{in=1}^4 C_A(in/XY) \right)$$

$$\eta_i^{YZ}(i) = \frac{4}{3} \left(\bar{C}_A(i) - \frac{1}{4} \sum_{in=1}^4 C_A(in/YZ) \right) = \frac{1}{3} \left(C_A(i) + \frac{1}{4} \sum_{in=1}^{12} C_A(in) - \sum_{in=1}^4 C_A(in/YZ) \right)$$

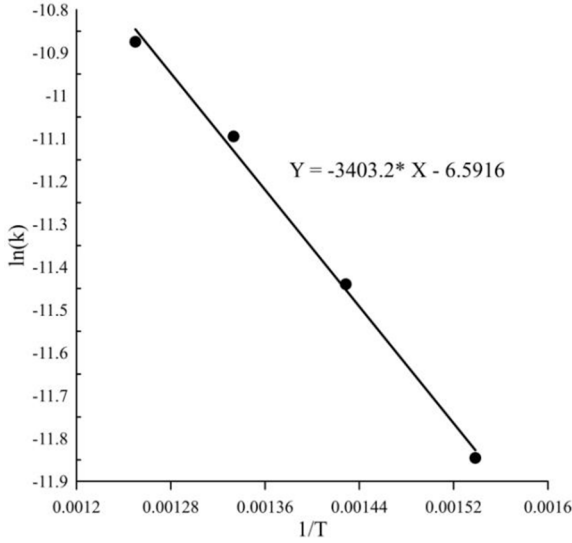


Fig. 8. Arrhenius law for the parabolic growth rate constant (phase A3B in A-AB couple).

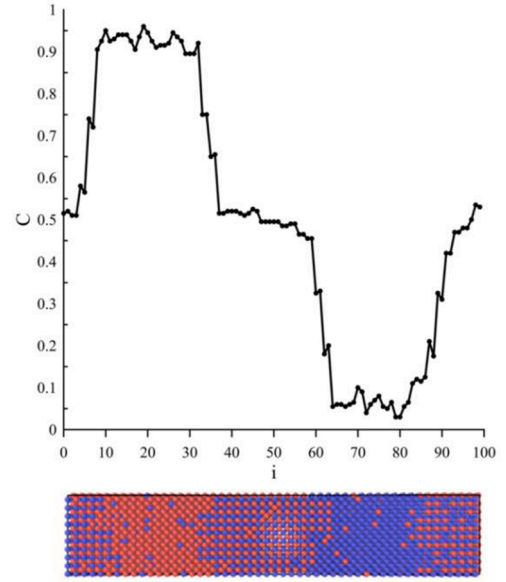


Fig. 9. Typical concentration profile (averaged over YZ-planes) and a corresponding snapshot of the cross-section obtained by MC-simulations during diffusion and ordering in the BCC-couple A-B.

$$\eta_i^{ZX}(i) = \frac{4}{3} \left(\bar{C}_A(i) - \frac{1}{4} \sum_{in=1}^4 C_A(in/ZX) \right) = \frac{1}{3} \left(C_A(i) + \frac{1}{4} \sum_{in=1}^{12} C_A(in) - \sum_{in=1}^4 C_A(in/ZX) \right)$$

If site “i” belongs to minority sublattice, then:

$$\eta_{ii}(i) = \frac{C_B(i) - \frac{C_B(i)+4 \sum_{m=1}^{12} C_B(im)}{4}}{1 - 1/4} = \frac{\frac{C_A(i)+4 \sum_{m=1}^{12} C_A(im)}{4} - C_A(i)}{1 - 1/4}$$

In general, taking into account the possibilities of antiphase domains choice,

$$\eta^{L12}(i) = \max\{abs(\eta_i^{XY}(i)), abs(\eta_i^{YZ}(i)), abs(\eta_i^{ZX}(i)), abs(\eta_{ii}(i))\} \quad (7)$$

Below we investigate diffusion and ordering in the diffusion couples oriented along axis X, we average local concentrations and local order parameters over each atomic plane YZ. The typical sizes of diffusion couples are: 100 atomic planes along axis X (with periodic boundary conditions along X), 20 planes along axis Y, and the same along axis Z.

In Sections 3 and 4 we use the direct atomic exchanges mechanism and Metropolis algorithm with the probability of an atom jumping from site “i” to site “j” is determined by the dependence:

$$p_{i \rightarrow j} = \begin{cases} 1, & (\Delta E \leq 0) \\ \exp\left(-\frac{\Delta E}{kT}\right), & (\Delta E > 0) \end{cases}$$

$\Delta E = E_j - E_i$, E_i and E_j – system energies before and after the jump, k – Boltzmann constant; T – system temperature.

3. An account of interactions within the second coordination shell

3.1. FCC-couple

For an illustration of the second shell influence, we chose the interaction energies within first and second coordination shells. Contrary to KMF (mean-field approach [5–8]), in which the activation energies are calculated as the differences between some common saddle-point energy and the energy of configuration before jump, in Metropolis algorithm of Monte Carlo the exchange probabilities are determined only by the difference of configuration energies after and before exchange. Therefore, in our algorithm, the evolution is determined only by mixing energies (Contrary to this, in [5–8] the evolution depends also on the so-

Table 1

Comparison of growth parameters for single-phase growth in the incremental couple and for competitive simultaneous growth.

Activation energies and growth constants at fixed temperature for single-phase growth in the incremental couples A-AB and A3B-AB3	Activation energies and growth constants at fixed temperature for simultaneous growth of both phases in the couple A-AB3
$Q_{A3B}/k_B = 3403K$	$Q_{A3B}/k_B = 2355K$
$Q_{AB}/k_B = 3512K$	$Q_{AB}/k_B = 6162K$
$T = 750 K$	$k_{A3B} = 7.26 \cdot 10^{-6} MCS^{-1}$
$k_{A3B} = 1.52 \cdot 10^{-5} MCS^{-1}$	$k_{AB} = 2.52 \cdot 10^{-6} MCS^{-1}$
$k_{AB} = 7.67 \cdot 10^{-6} MCS^{-1}$	

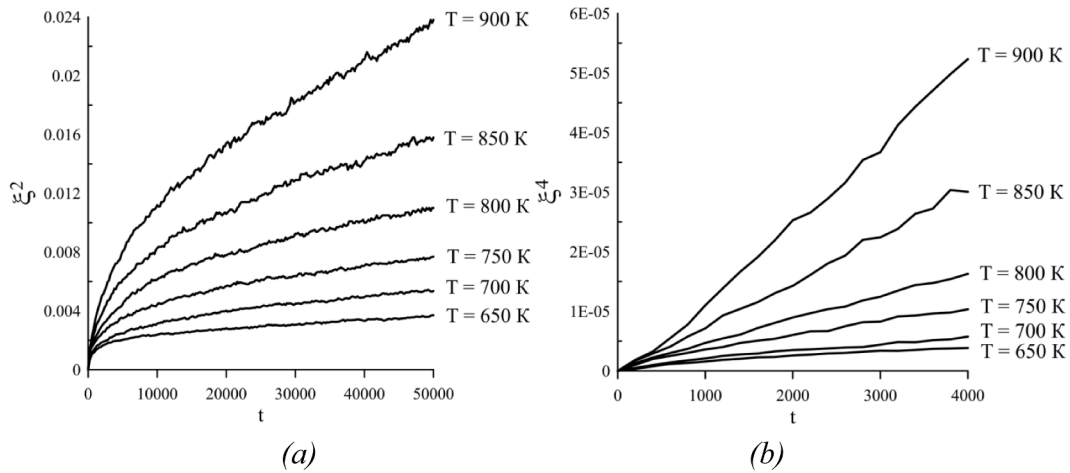


Fig. 10. (a) Dependencies of squared number ξ^2 of sites with overcritical local order parameter, on Monte Carlo Steps for the growth of B2 phase AB in BCC-diffusion couple A-B at various temperatures. (b) dependencies ξ^4 versus t at the initial stage of phase formation.

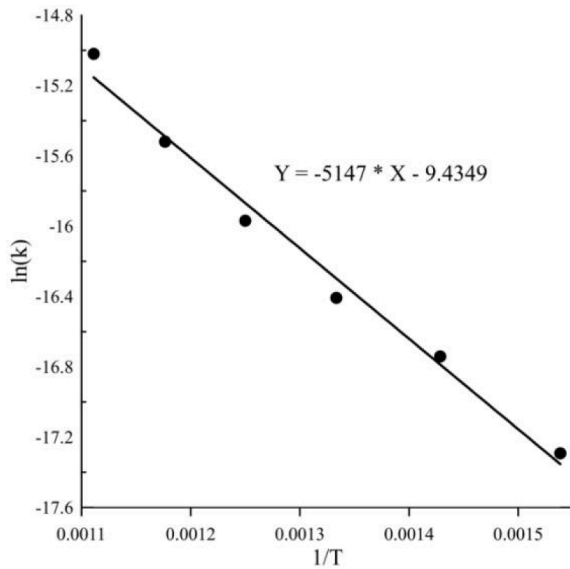


Fig. 11. Arrhenius law for the parabolic growth rate constant (phase AB with B2-structure in A-B bcc-couple).

called asymmetry parameter $(V_{AA} - V_{BB})/kT$. Thus, we take, $V_{mix}^I = -2.9 \cdot 10^{-21} J$, $V_{mix}^{II} = +6.76 \cdot 10^{-21} J$ and temperature interval from 650 K to 950 K. Note that mixing energy within the second shell is positive.

3.1.1. Equilibrium properties

We started with the construction of phase diagram by direct MC-simulation (Metropolis algorithm with direct exchanges) of equilibria in the diffusion couples, A-A3B, A3B-AB, AB-AB3 and AB3-B at various temperatures – the result is shown at Fig. 3 – it is qualitatively similar to analogic kinetic mean-field simulations in [5] but differ, of course, since in MC-simulations the short-range order (correlations between probabilities) is implicitly taken into account.

If one forgets for a while about correlations and short-range order, the Bragg-Williams approximation for such alloy gives the following typical dependences of Gibbs energy per atom $g(T, C, \eta^{opt}(T, C))$ as a function of composition and of optimized order at each composition:

3.1.2. Kinetics of intermediate phase formation

We simulated simultaneous ordering and phase formation in the couples A-AB (with the formation of single ordered intermediate phase

A3B), A3B-AB3 (with the formation of single ordered intermediate phase AB), and AB-AB3 (with the formation of two competing ordered intermediate phases A3B and AB). Results for every diffusion couple were obtained as average over the ensemble of 10 tests.

Corresponding transient profiles are shown at Fig. 5a,b and Fig. 6. Each concentration plateau corresponds to phase, sharp steps between plateau correspond to two-phase regions (gaps). Spike downwards at Fig. 5b corresponds to the antiphase boundary between two antiphase domains of $L1_0$ -phase. Snapshots of sites occupancy by A (red) and B (blue) within certain cross-sections are also shown.

In general, the volume of the ordered phase can be found from the width of the concentration plateau, if the phase grows layer by layer. If not, then a more safe way is to count the number of sites with local order parameter higher than some threshold (critical) value. We choose $\eta_{cr} = 0.85$. So, to check the validity of parabolic law, we built the dependence of squared fraction ξ^2 of sites with overcritical local order parameter ($\eta > \eta_{cr}$), on time (in Monte Carlo Steps). Such dependencies at various temperatures are shown in Fig. 7.

After some initial non-parabolic period, all these dependencies tend to $\xi^2 = kt$, where the growth constant k satisfies the Arrhenius law in Eq. (8) (Fig. 8):

$$\ln(k) = -\frac{Q_{A3B}}{k_B} \frac{1}{T} + const \quad (8)$$

Similar computer annealing was made for the single-phase AB ($L1_0$) growth in the incremental couple A3B-AB3, and for the simultaneous growth of two phases (A3B ($L1_2$) and AB($L1_0$)) in the couple A-AB3.

As expected, (see Table 1), the single-phase growth without competition is faster than competitive simultaneous growth with the neighboring phase. At the initial stage, this competition may even fully suppress one of two phases, as described in [1]. Phase suppression and competition will be simulated with MC in more details elsewhere. (Within a rough mean-field model it was done, for example, in [8]).

3.2. BCC-couple

Here we used the same parameters, as for FCC lattice: $V_{mix}^I = -2.9 \cdot 10^{-21} J$, $V_{mix}^{II} = +6.76 \cdot 10^{-21} J$ within temperature interval from 650 K to 900 K. Typical concentration profile demonstrating the growth of AB-phase in A-B couple, is shown in Fig. 9.

One can see in Figs. 10, 11 that the transition to the parabolic regime for B2 phase growth takes more time (in MCS), and Arrhenius law is not that ideal.

At the initial stages (less than 5000 MC-steps) the growth law is

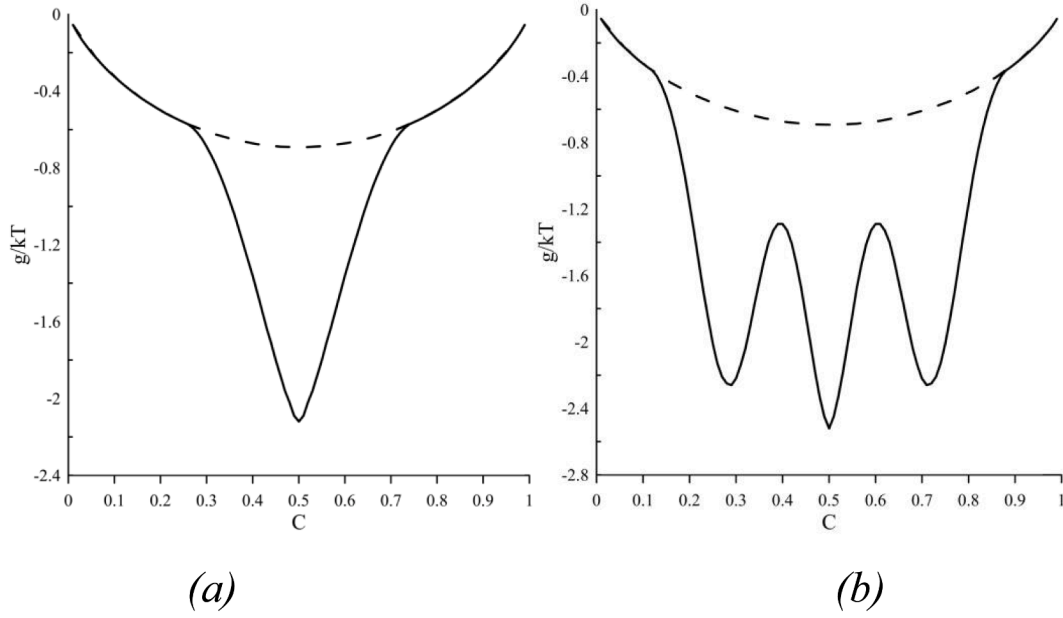


Fig. 12. Typical dependence $g(C,T)/kT$ with composition-dependent interaction (a) of type (9a) with $ER = 8.5$, $\alpha = 20$ and (b) of type (9b) with, $ER_1 = ER_3 = 80$, $ER_2 = 30$, $\alpha_1 = \alpha_2 = \alpha_3 = 100$.

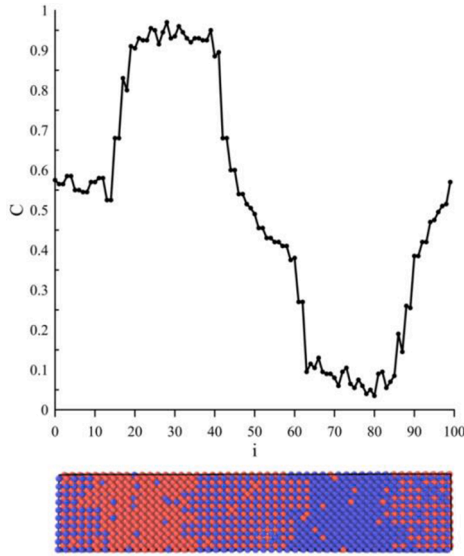


Fig. 13. Concentration profile (averaged over each YZ atomic plane) and a corresponding snapshot of the cross-section, obtained by MC-simulation of BCC-couple A-B with composition-dependent interactions according to Eqs. (9)–(11).

closer to $\xi^4 \approx kt$ (Fig. 10b). Note that similar time dependence can be observed for the layer growth via grain-boundary diffusion with simultaneous lateral parabolic grain growth [15].

4. An account of interactions depending on local surrounding

4.1. General equations

Let us assume that the interaction energy between nearest neighbors of different sorts (A and B) sharply depends on the composition of the surrounding cluster and becomes most intensive if this composition is equal to stoichiometric value. For example, it can be single gauss-like dependence, if we want to distinguish a single intermediate phase with stoichiometric composition C_{IMC} ,

$$\frac{V_{mix}}{k_B T} = -\frac{ER}{Z} \exp(-\alpha(C_{cluster} - C_{IMC})^2) \quad (9a)$$

or, it can be the superposition of 3 gauss-like dependences, if we want to distinguish 3 intermediate phases, say, A3B, AB, AB3:

$$\begin{aligned} \frac{V_{mix}}{k_B T} = & -\frac{ER_1}{Z} \exp(-\alpha_1(C_{cluster} - 1/4)^2) - \frac{ER_2}{Z} \exp(-\alpha_2(C_{cluster} - 1/2)^2) \\ & - \frac{ER_3}{Z} \exp(-\alpha_3(C_{cluster} - 3/4)^2) \end{aligned} \quad (9b)$$

Here $ER = \frac{Z|E_{mix}|}{k_B T}$ is the reduced mixing energy for stoichiometric composition. If one substitutes interaction energy Eq. (9a) into the Bragg-Williams approximation, it gives the typical dependencies shown in Fig. 12a,b.

Defining the case of Monte Carlo simulation, we provide the precise definition of the surrounding cluster composition in Eq. (10).

$$C_{cluster} = \frac{\bar{C}(i) + \bar{C}(j)}{2} \quad (10)$$

the average composition of the cluster consisting of two interacting atoms in the neighboring sites “i”, “j” and their nearest neighbors, $\bar{C}(i)$, $\bar{C}(j)$ — mean concentrations prescribed to each of two neighboring sites.

In the case of B2 structure at BCC lattice we define mean concentration according to Eq. (11a).

$$\bar{C}(i) = \frac{C(i) + \frac{1}{8} \sum_{in=1}^8 C(in)}{2}, \quad \bar{C}(j) = \frac{C(j) + \frac{1}{8} \sum_{jn=1}^8 C(jn)}{2} \quad (11a)$$

In case of L1₂ and L1₀ structures at FCC lattice we define mean concentration according to Eq. (11b).

$$\bar{C}(i) = \frac{C(i) + \frac{1}{4} \sum_{in=1}^{12} C(in)}{4}, \quad \bar{C}(j) = \frac{C(j) + \frac{1}{4} \sum_{jn=1}^{12} C(jn)}{4} \quad (11b)$$

4.2. Simulation of AB -layer growth in BCC diffusion couple

Applying Metropolis algorithm with interactions calculated according to eqs. (9)–(11), we get the formation and growth of B2-phase – see Fig. 13.

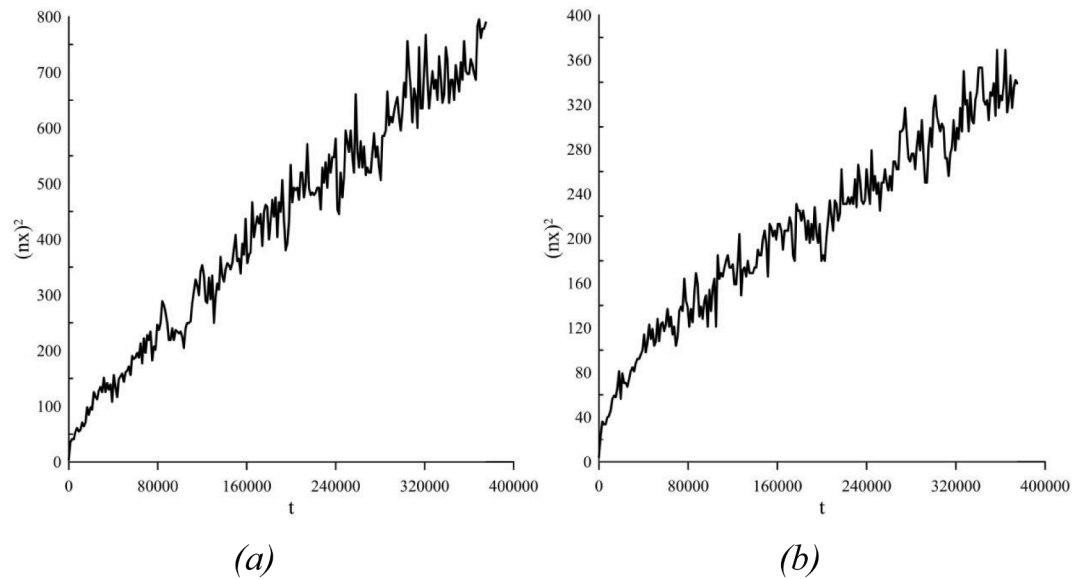


Fig. 14. The squared number of planes with an average concentration within the range 0.425–0.575 versus the number of Monte Carlo Steps a) $ER = 8.5$; b) $ER = 10$.

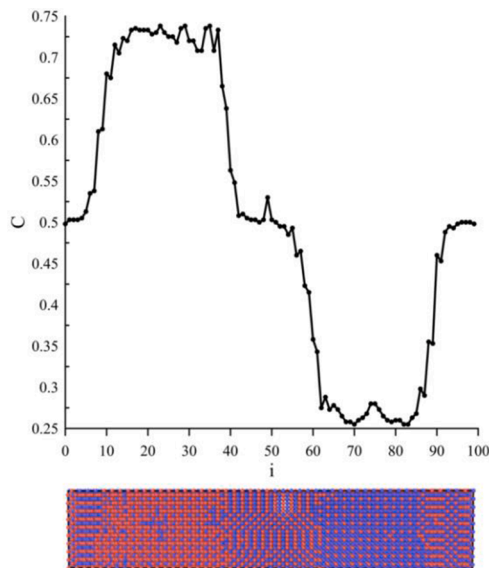


Fig. 15. Concentration profile (local concentrations averaged over planes YZ) and a snapshot of the cross-section for the transient moment of interdiffusion in A3B-AB3 couple. Parameters: $ER_1 = ER_2 = ER_3 = 60$, $\alpha_1 = \alpha_2 = \alpha_3 = 110$.

Growth kinetics was measured by counting the number of planes with average concentration within the range (0.425–0.575) (Fig. 14).

4.3. Simulation of IMC growth and competition in FCC diffusion couples.

We simulated IMC growth in FCC couples, introducing composition-dependent interactions according to Eq. (11b) with parameters $ER_1 = ER_2 = ER_3 = 60$, $\alpha_1 = \alpha_2 = \alpha_3 = 110$.

Couple A3B-AB3. Single ordered intermediate phase AB with structure $L1_0$ is formed and grows. The transient composition profile and a snapshot of the lattice are shown at Fig. 15.

Couple A-AB. Single ordered intermediate phase A3B with structure $L1_2$ is formed and grows. The composition profile and snapshot of the lattice are shown in Fig. 16.

Couple A-AB3. Two ordered intermediate phases A3B with structure

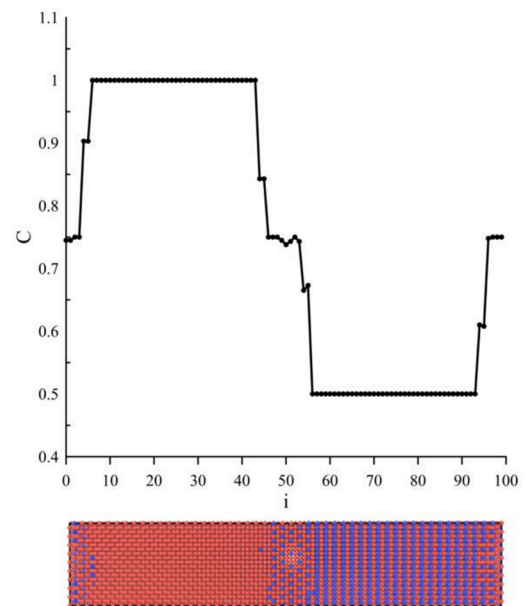


Fig. 16. Concentration profile (local concentrations averaged over planes YZ) and a snapshot of the cross-section for the transient moment of interdiffusion in A-AB couple. Parameters: $ER_1 = ER_2 = ER_3 = 60$, $\alpha_1 = \alpha_2 = \alpha_3 = 110$.

$L1_2$ and AB with structure $L1_0$ are formed and grow simultaneously. The composition profile and snapshot of the lattice are shown in Fig. 17.

Time dependencies (in Monte Carlo Steps) of phase thicknesses are shown in Fig. 18. They can be approximated by the parabolic law with the non-zero initial thickness (which may mean fast lateral growth at the initial stage): $\Delta X^2 = \Delta X_0^2 + kt$.

5. Simulation of phase growth and competition by RTA-algorithm

The questionable issue of previous Sections 3,4 is the use Metropolis algorithm and of direct atomic exchange mechanism for description of “time” dependencies of the phase width and total order. So far in this paper, our “time” was just the number of MC-steps. Strictly speaking, to

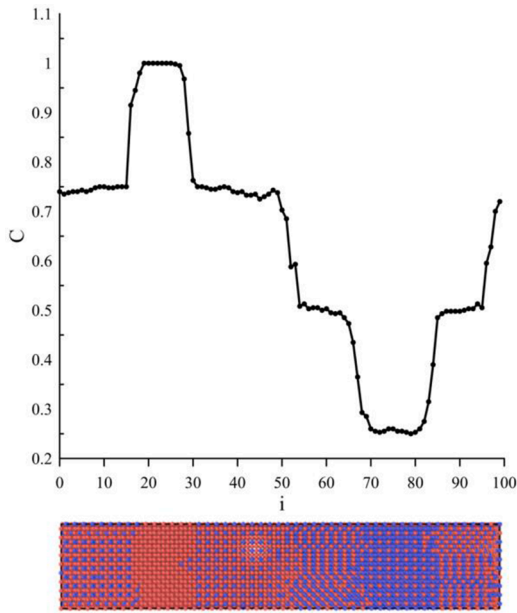


Fig. 17. Concentration profile (local concentrations averaged over planes YZ) and a snapshot of the cross-section for the transient moment of interdiffusion in A-AB3 couple. The plateau at concentrations of about 0.75 and 0.5 correspond to two ordered phases growing simultaneously. Parameters: $ER_1 = ER_2 = ER_3 = 60$, $\alpha_1 = \alpha_2 = \alpha_3 = 110$.

describe the more realistic development in real time, one needs the kinetic Monte Carlo which is realized usually by Residence-Time Algorithm (RTA).

Indeed, in general, Metropolis algorithm may result in distortion of real time rates, but commonly it gives the correct sequence of events. According to G.Murch, “Although Metropolis transition probability is not particularly realistic for a diffusion process, the number of Monte Carlo jump attempts scales transparently to real time” [23]. RTA works well for vacancy mechanism, when vacancy chooses one of 12 (in FCC) or one of 8 (in BCC) possible evolution paths. In case of atomic exchange mechanism, the number of possible exchanges which compete within the system, is enormous. Usually, RTA-calculations take more time and memory. Moreover, if one uses a single vacancy per system, it can be trapped for some time within some phase region (see below), and to have the realistic rate observation, one should continue the simulations much longer, to satisfy the ergodicity criterion.

We recalculated the diffusion, phase formation and ordering in three FCC diffusion couples, (A-AB and A-AB3 with constant interactions within two coordination shells, and A3B-AB3 with composition exponentially-dependent interaction within only first coordination shell) using the following standard equations for the probabilities of vacancy jumps Eq. (12) and for increment of real time after each jump Eq. (13):

$$p(i \rightarrow in) = \frac{\nu_0(in) \exp\left(-\frac{Q}{kT}\right) \exp\left(-\frac{E_{after}(i \rightarrow in) - E_{before}}{2kT}\right)}{\sum_{im=1}^Z \nu_0(im) \exp\left(-\frac{Q}{kT}\right) \exp\left(-\frac{E_{after}(i \rightarrow im) - E_{before}}{2kT}\right)}$$

$$= \frac{\nu_0(in) \exp\left(-\frac{E_{after}(i \rightarrow in) - E_{before}}{2kT}\right)}{\sum_{im=1}^Z \nu_0(im) \exp\left(-\frac{E_{after}(i \rightarrow im) - E_{before}}{2kT}\right)} \quad (12)$$

$$\Delta t(i \rightarrow in) = \frac{1}{\exp\left(-\frac{Q}{kT}\right) \sum_{im=1}^Z \nu_0(im) \exp\left(-\frac{E_{after}(i \rightarrow im) - E_{before}}{2kT}\right)} \quad (13)$$

Here “i” is a position of vacancy before its jump, “in” is one of Z

nearest neighboring site, to which vacancy may jump, $\nu_0(im)$ is an attempt frequency (to exchange with vacancy) by atom situated in neighboring site “im”, Q — common part of activation energy for all possible jumps, E_{before} and $E_{after}(i \rightarrow im)$ are the energies of the system before vacancy jump and after its exchange with atom at site “im”. Energies were calculated as in previous sections. Q was taken as $10^{-19}J$. All attempt frequencies were take the same: $\nu_0(im) = \nu_0$, and non-dimensional time $t = \nu_0 \cdot \text{realtimewas}$ used.

Fig. 19 appears to be similar (except scale, of course) to Fig. 7a, obtained by Metropolis algorithm with direct atomic exchanges.

According to Fig. 20, growth of domains of newly formed L10 ordered phase initially suppresses the initial weak order L12 (formed just at the initial contact planar interface). When the fast growing phase AB with L10 order consumes all initial pure B, the phase AB becomes marginal, it cannot grow further and is consumed by A3B phase which starts growing. If compare with the same results obtained by Metropolis algorithm with direct atomic exchanges shown in Fig. 7b,c we can notice that visible initial suppression of initial weak order phase L12 by newly formed L10 is absent. Moreover, phase L10 in case of vacancy mechanisms grows faster than L12 and in case of direct exchange mechanism — vice versa. One can imagine several reasons for such difference between two algorithms. One of them may be related to the anisotropy of AB-ordered phase growth. In our simulations with vacancy mechanism all domains of the AB-phase had atomic planes of A and B perpendicular to the interface (snapshot at Fig. 20). In our simulations with direct exchange mechanism we observe planes of A and B parallel to interface as well as perpendicular (snapshot at Fig. 17). Interdiffusion along the domain with atomic planes A and B perpendicular to interface, is faster than for parallel orientation [24].

According to Fig. 21, growth of AB phase is very irregular in time (like “stop-and-go” process). As shown in video (Supplementary material), such behavior is related to temporal trapping of single vacancy inside one of two intermediate phase layers (we have two layers instead of one, due to periodic boundary conditions). We did not have this problem with direct exchange mechanism. To solve this problem one should introduce several vacancies (but then one should be careful about their interaction because of vacancy supersaturation) or just make much longer annealing with averaging over time intervals.

Thus, the results of RTA for vacancy mechanism and for Metropolis exchange mechanism are qualitatively similar in the case of single-phase growth but differs significantly in the case of phase competition during two intermediate phase formation. At that, one must remember that the vacancy mechanism is adequate for description of tracer diffusion but not very realistic in common simulation of interdiffusion and phase growth, because it does not take into account the vacancy sinks and sources and, respectively, dislocation climb and equalizing of components’ fluxes by the Kirkendall effect.

6. Discussion and conclusions

In this paper, we suggest and compare two major “tricks” — account of interactions with second coordination shell, and account of non-linear composition-dependent interaction within the first coordination shell. Both of them demonstrate the possibilities of distinguishing the phase layers with characteristic concentration plateau, ordering, and growth. The first trick is not that new, but almost not used, so far, for the ordered phase formation modeling in reactive diffusion (see [8]). Second trick — sharp concentration dependence of pair interactions — seems to be really new, we hope that it might be useful for the diffusion-ordering-reaction simulation community.

No doubt, in the case of long annealing and parabolic growth of intermediate phases one may use Monte Carlo just as one level of multi-scale modeling [14]: Molecular statics and dynamics (and may be DFT) give activation energies and preexponential factors for the atomic (actually, vacancy) jumps for all possible configurations, Monte Carlo

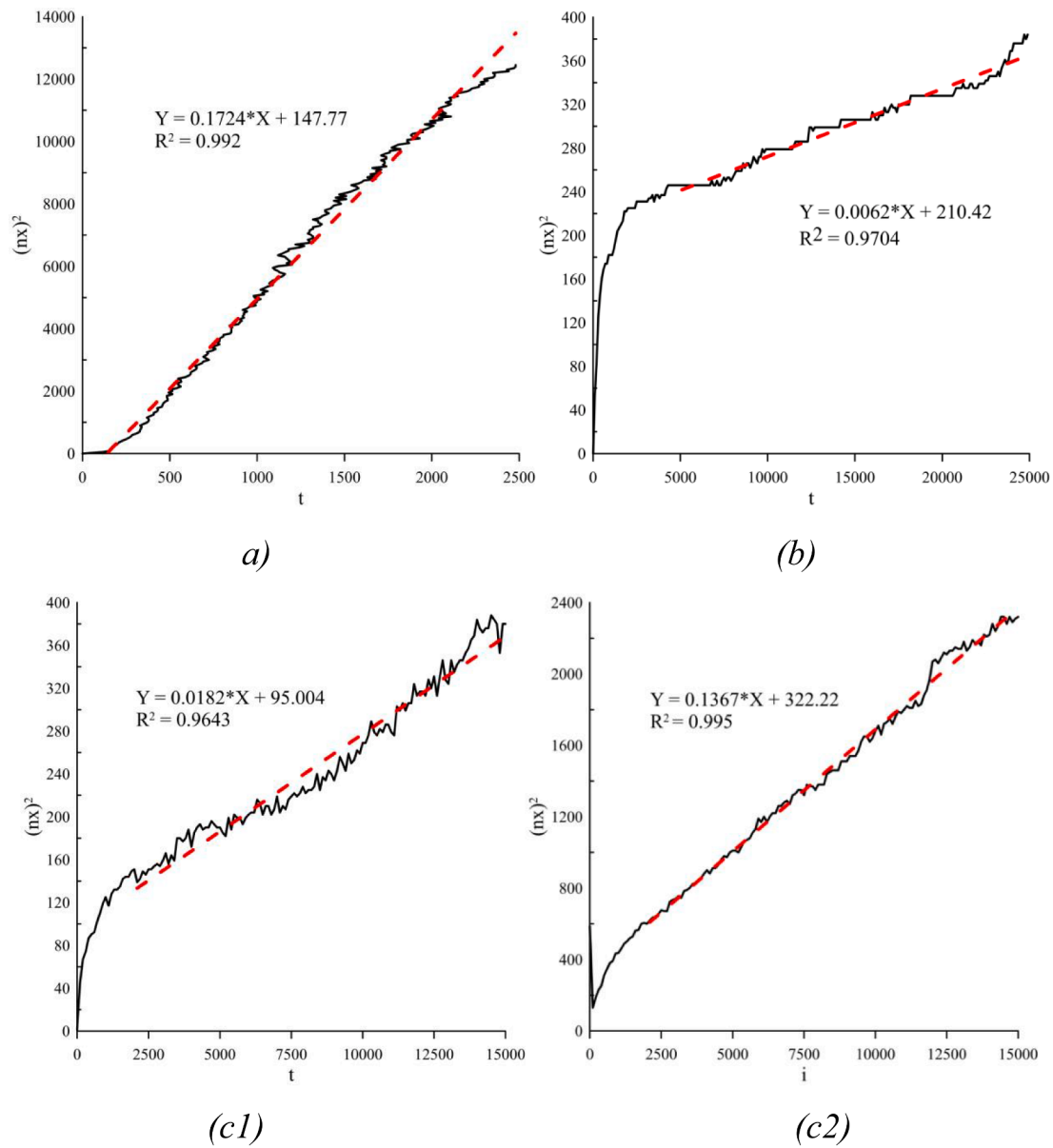


Fig. 18. Time dependencies of the phase thicknesses for cases shown in Figs. 15–17: (a) for single-phase growth of $L1_0$ structure in A3B-AB3 couple; (b) for single-phase growth of $L1_2$ structure in A-AB couple; (c1) for growth of $L1_0$ structure with the simultaneous growth of $L1_2$ in the couple A-AB3; (c2) for growth of $L1_2$ structure with the simultaneous growth of $L0_2$ in the couple A-AB3. Parameters: $ER_1 = ER_2 = ER_3 = 60$, $\alpha_1 = \alpha_2 = \alpha_3 = 110$.

uses this information for simulation of tracer atoms at given ordered structures and, possibly, of vacancy wind effects. This information is then used by phenomenological theory to calculate the Kirkendall effect and interdiffusion fluxes. At the very end, in coarsened space and time scales, these interdiffusion fluxes are incorporated into the Stefan problem of simultaneously growing phase layers.

Such an idealistic picture is not very reliable in respect to known problems of stress generation and relaxation, void formation [18,19], migration, and pinning by moving interfaces [20], etc. We believe that the most challenging problem is still the initial stage when competing ordering and competing phase formation proceed simultaneously. In this case, one needs some united scheme that treats ordering, diffusion, and phase growth holistically. Solving this problem with vacancy mechanism, without appropriate tools to treat Kirkendall shift within Monte Carlo, seems too complicated problem at this moment. On the other hand, the action of Kirkendall effect, remaining gradients of nonequilibrium vacancies and stresses eventually equalize the opposite fluxes of A and B in the laboratory (Matano) reference frame. Therefore,

the exchange mechanism in Monte Carlo simulation of reactive phase growth is not that “old-fashioned”. Nevertheless, we try also the vacancy mechanism with RTA-algorithm, though within the idealized model of rigid lattice. In both algorithms (Metropolis for direct exchanges and RTA for vacancy exchanges with atoms) both our tricks for intermediate phase formation and competition work effectively providing reasonable concentration plateau for the growing intermediate phases, distinct concentration steps at the interfaces, parabolic growth laws after nucleation stage.

Actually, interdiffusion in binary alloy by vacancy mechanism without vacancy sinks and sources leads to Nernst-Planck-type expression Eq. (14) for effective interdiffusion coefficient in terms of partial diffusivities:

$$\tilde{D} = \frac{D_A D_B}{C_A D_A + C_B D_B} \quad (14)$$

where D_A, D_B are the products of tracer diffusivities and thermodynamic factor [25,26,1].

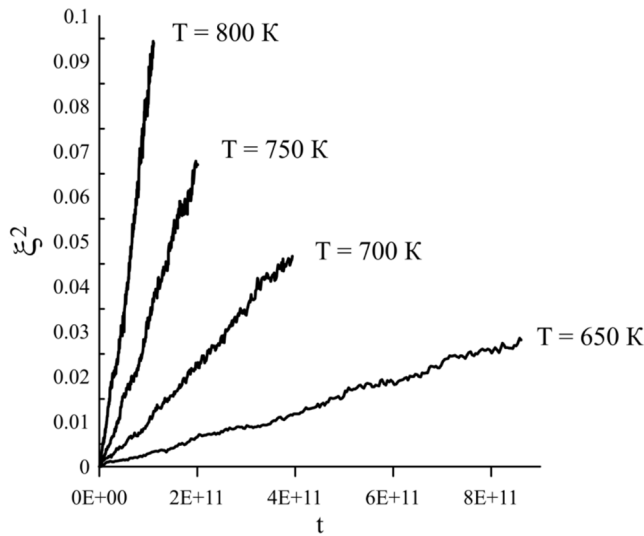


Fig. 19. Squared fraction of sites with local L_{12} order parameter above 0.85 as a function of time in simulation of interdiffusion between pure A and ordered AB by RTA-algorithm with vacancy mechanism. (Case of constant pair interaction energies within two coordination shells).

Since tracer diffusivities are typically proportional to the vacancy-atoms exchange frequencies and to the vacancy concentration, one might expect that the frequency of effective atomic exchanges is related (at least approximately) to frequencies of vacancy exchanges with A and B in Eq. (15):

$$\nu^{ef} = \frac{C_V \nu_{AV} \nu_{BV}}{C_A \nu_{AV} + C_B \nu_{BV}} \quad (15)$$

(Here all C are the non-dimensional fractions – probabilities for site to be occupied by A,B or vacancy)

In real alloys the density of sinks and sources of vacancies is sufficient. This leads to Kirkendall shift and to the Darken expression for interdiffusion coefficient (later modified by Manning with account of vacancy wind effect). Therefore, if one expects to take into account the Kirkendall shift, then one must relate (at least approximately) effective exchange rate to the atom-vacancy exchange frequencies in the different way Eq. (16):

$$\nu^{ef} = C_V (C_B \nu_{AV} + C_A \nu_{BV}) \quad (16)$$

The next step in applications of the suggested algorithms can be related to nucleation of ordered IMC in homogeneous solution and in the sharp concentration gradients. (Thorough MC study of disordered phase nucleation can be found in [21].) Another important direction of further research would be checking the applicability of the idea of concentration-dependent nonlinear interactions to the recently developed stochastic version of mean-field approach [7,8,22].

CRedit authorship contribution statement

Viktoriiia Pasichna: Methodology, Software, Validation, Investigation, Resources, Data curation, Visualization. **Andriy Gusak:** Conceptualization, Formal analysis, Writing - original draft, Supervision, Project administration, Funding acquisition.

Declaration of Competing Interest

The authors declare that they have no known competing financial interests or personal relationships that could have appeared to influence the work reported in this paper.

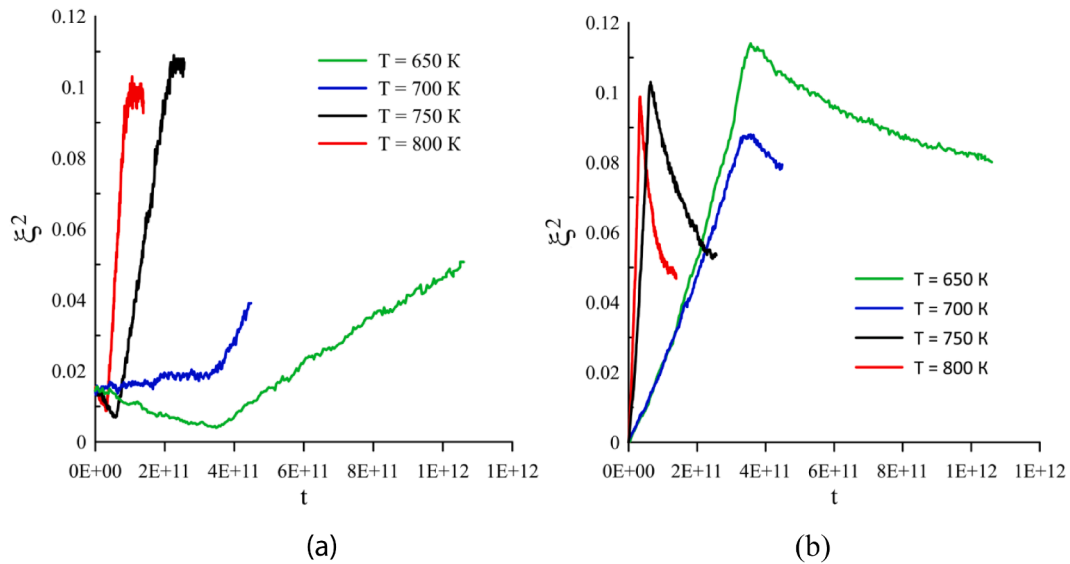


Fig. 20. Squared fraction of sites with (a) local L_{12} order parameter and with (b) local L_{10} order parameter above 0.85 as the functions of time in simulation of interdiffusion between pure A and ordered AB3 by RTA-algorithm with vacancy mechanism. (Case of constant pair interaction energies within two coordination shells).

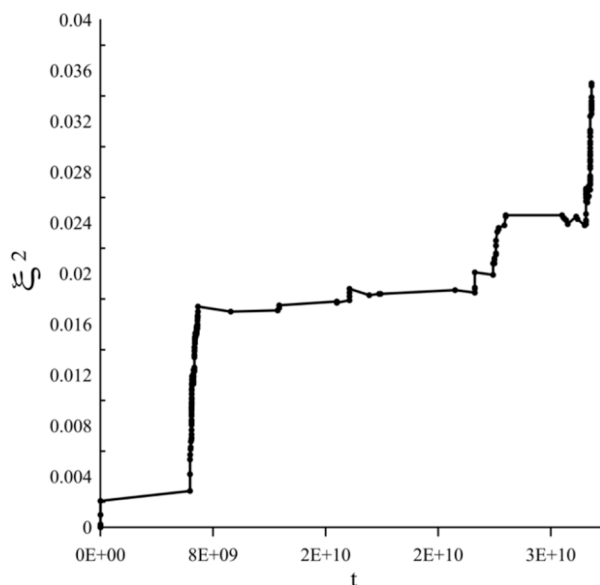


Fig. 21. Squared fraction of sites with local $L1_0$ order parameter above 0.85 as a function of time in simulation of interdiffusion between ordered A3B and ordered AB3 by RTA-algorithm with vacancy mechanism. (Case of composition dependent interaction energies within first coordination shell) Parameters: $ER_1 = ER_2 = ER_3 = 60$, $\alpha_1 = \alpha_2 = \alpha_3 = 110$.

Acknowledgement

Ukraine (project 0118U003861).

This work was supported by the Ministry of Education and Science of

Attachment A. Influence of perturbations on the simulation results.

Change of the slope of the linear dependence “squared thickness / time (in percents)

T	small perturbations of initial atomic distribution with unchanged mean composition: random variation of initial atomic disorder within phase layer AB with the constant order parameter	small perturbations of initial shape of contact: interface roughness by introducing steps with the height of 4 interplanar distances	small perturbations of initial compositions in the diffusion couple: in the couple A-AB we change 100% A by 98% (within solubility limit)
650 K	-2.3%	1.0%	1.8%
700 K	3.2%	2.3%	3.2%
750 K	-0.0053-0.5%	2.1%	0.8%
800 K	2.0%	4.6%	5.7%

Appendix A. Supplementary data

Supplementary data to this article can be found online at <https://doi.org/10.1016/j.commat.2020.110114>.

References

- [1] A.M. Gusak, T.V. Zaporozhets, Y.O. Lyashenko, S.V. Kornienko, M.O. Pasichnyy, A. S. Shirinyan, Diffusion-controlled solid state reactions: in alloys, thin films and nanosystems, John Wiley & Sons, 2010. ISBN: 978-3-527-40884-9.
- [2] G.E. Murch, I.V. Belova, in: Handbook of solid state diffusion, Volume 1, Elsevier, 2017, pp. 435–448, [10.1016/B978-0-12-804287-8.00009-9](https://doi.org/10.1016/B978-0-12-804287-8.00009-9).
- [3] J. Betlej, P. Sowa, R. Kozubski, G.E. Murch, I.V. Belova, Self-diffusion in a triple-defect A-B binary system: Monte Carlo simulation, Comput. Mater. Sci. 172 (2020) 109316, <https://doi.org/10.1016/j.commat.2019.109316>.
- [4] R. Kozubski, Long-range order kinetics in Ni3Al-based intermetallic compounds with L12-type superstructure, Prog. Mater. Sci. 41 (1-2) (1997) 1–59.
- [5] G. Martin, Atomic mobility in Cahn’s diffusion model, Phys. Rev. B 41 (4) (1990) 2279–2283.
- [6] Z. Erdélyi, D.L. Beke, A. Taranovskyy, Dissolution and off-stoichiometric formation of compound layers in solid state reactions, Appl. Phys. Lett. 92 (13) (2008) 133110, <https://doi.org/10.1063/1.2905334>.
- [7] N.V. Storozhuk, K.V. Sopiga, A.M. Gusak, Mean-field and quasi-phase-field models of nucleation and phase competition in reactive diffusion, Phil. Mag. 93 (16) (2013) 1999–2012.
- [8] A. Gusak, T. Zaporozhets, N. Storozhuk, Phase competition in solid-state reactive diffusion revisited—Stochastic kinetic mean-field approach, J. Chem. Phys. 150 (17) (2019) 174109, <https://doi.org/10.1063/1.5086046>.
- [9] Paul, A., & Divinski, S. (Eds.). (2017). Handbook of Solid State Diffusion: Volume 2: Diffusion Analysis in Material Applications. Elsevier. ISBN: 978-0-12-804548-0.
- [10] A. Portavoce, G. Tréglia, Physical origin of thickness-controlled sequential phase formation during reactive diffusion: atomistic modeling, Phys. Rev. B 82 (20) (2010), 205431, <https://doi.org/10.1103/PhysRevB.82.205431>.
- [11] A.M. Gusak, N. Storozhuk, Two remarks on Wagner integrated diffusion coefficient, Metallophys. Adv. Technol. 41 (5) (2019) 583–593.
- [12] M. Pasichnyy, A. Gusak, Modeling of phase competition and diffusion zone morphology evolution at initial stages of reaction diffusion, in: Defect and Diffusion Forum (Vol. 237, pp. 1193–1198). Trans Tech Publications Ltd., 2005, DOI: <https://doi.org/10.4028/www.scientific.net/DDF.237-240.1193>.
- [13] B. Gajdics, J.J. Tomán, H. Zapolsky, Z. Erdélyi, G. Demange, A multiscale procedure based on the stochastic kinetic mean field and the phase-field models for coarsening, J. Appl. Phys. 126 (6) (2019) 065106, <https://doi.org/10.1063/1.5099676>.
- [14] J.L. Bocquet, On-the-fly evaluation of diffusional parameters during a Monte Carlo simulation of diffusion in alloys: A challenge. In Defect and Diffusion Forum (Vol.

- 203, pp. 81-112). Trans Tech Publications Ltd., 2002 DOI: <https://doi.org/10.4028/www.scientific.net/DDF.203-205.81>.
- [15] Y. Liu, L.i. Pu, A. Gusak, X. Zhao, C. Tan, K.N. Tu, Ultra-thin intermetallic compound formation in microbump technology by the control of a low Zn concentration in solder, *Materialia* 12 (2020) 100791, <https://doi.org/10.1016/j.mtla.2020.100791>.
- [16] Piotr Sowa. (2017) Atomistic simulation of mass transport phenomena in inhomogeneous intermetallic systems, (2017), PhD thesis (Krakow, Jagiellonian University).
- [17] V.M. Bezpachuk, R. Kozubski, A.M. Gusak, Simulation of the tracer diffusion, bulk ordering, and surface reordering in F.C.C. structures by kinetic mean-field method, *Usp. Fiz. Met.* 18 (3) (2017) 205–233.
- [18] V.A. Baheti, S. Kashyap, P. Kumar, K. Chattopadhyay, A. Paul, Bifurcation of the Kirkendall marker plane and the role of Ni and other impurities on the growth of Kirkendall voids in the Cu–Sn system, *Acta Mater.* 131 (2017) 260–270.
- [19] A.M. Gusak, N.V. Storozhuk, Competition of K and F sinks during void formation, *Phys. Metals Metallogr.* 114 (3) (2013) 197–206.
- [20] A. Gusak, T. Zaporozhets, J. Janczak-Rusch, Kinetic pinning versus capillary pinning of voids at the moving interface during reactive diffusion, *Philos. Mag. Lett.* 97 (1) (2017) 1–10.
- [21] F. Soisson, G. Martin, Monte Carlo simulations of the decomposition of metastable solid solutions: transient and steady-state nucleation kinetics, *Phys. Rev. B* 62 (1) (2000) 203, <https://doi.org/10.1103/PhysRevB.62.203>.
- [22] T.V. Zaporozhets, A. Taranovskyy, G. Jáger, A.M. Gusak, Z. Erdélyi, J.J. Tomán, The effect of introducing stochasticity to kinetic mean-field calculations: Comparison with lattice kinetic Monte Carlo in case of regular solid solutions, *Comput. Mater. Sci.* 171 (2020), 109251, <https://doi.org/10.1016/j.commatsci.2019.109251>.
- [23] G.E. Murch, et al., Recent progress in the simulation of diffusion associated with hollow and Bi-metallic nanoparticles, *Diffus Fundam* 11 (2009) 42–51.
- [24] V. M. Bezpachuk, R. Kozubski, and A. M. Gusak, Simulation of the tracer diffusion, bulk ordering, and surface reordering in F.C.C. structures by kinetic mean-field method, *Usp. Fiz. Met.*, 18, No. 3: 205–233 (2017), doi: 10.15407/ufm.18.03.205; <https://doi.org/10.15407/ufm.18.03.205>, see also PhD thesis of V.Bezpachuk (2017), Odesa (Ukraine).
- [25] A.V. Nazarov, K.P. Gurov, Kinetic Theory of interdiffusion in binary system. Influence of non-equilibrium vacancies on interdiffusion, *Fiz. Met. Metalloved.* 37 (1974) 496–503.
- [26] K.P. Gurov, A.M. Gusak, A description of interdiffusion in alloys with an arbitrary capacity of vacancy sinks, *Fiz. Met. Metalloved.* 59 (6) (1985) 1062–1066.